ELSEVIER

Journal of Chromatography A, 849 (1999) 445–465

JOURNAL OF CHROMATOGRAPHY A

Kinetic study of the mass transfer of *S*-Tröger's base in the system cellulose triacetate and ethanol

Kanji Miyabe[a,b], Georges Guiochon[a,b,*]

[a]*Department of Chemistry, The University of Tennessee, Knoxville, TN 37996-1600, USA*
[b]*Division of Chemical and Analytical Sciences, Oak Ridge National Laboratory, Oak Ridge, TN 37831, USA*

Received 22 February 1999; received in revised form 19 April 1999; accepted 28 April 1999

Abstract

A recent study of the mass transfer kinetics of (−)- or *S*-Tröger's base (TB) between ethanol and microcrystalline cellulose triacetate (CTA) allows an analysis of the concentration dependence of the mass transfer rate coefficient (k_m). *S*-TB elutes before *R*-TB. The retention time of the both compounds decreases with increasing temperature. In this study, experimental data measured between 30 and 50°C were analyzed to provide information on the kinetics of several mass transfer processes which take place in the chromatographic column, i.e., axial and intraparticle dispersion, the fluid-to-particle mass transfer, and the kinetics of adsorption/desorption at the actual adsorption sites. Intraparticle diffusion has the dominant contribution to band broadening at high flow-rates. Both intraparticle diffusivity and the surface diffusion coefficient exhibit a small concentration dependence. The positive dependence of k_m on the concentration of *S*-TB seems to result from the properties of the adsorption/desorption kinetics and can be interpreted by considering the phase equilibrium properties. A quantitative analysis of the activation energy of the mass transfer kinetics of *S*-TB in the CTA column was also attempted.

Keywords: Mass transfer; Enantiomer separation; Tröger's base; Cellulose triacetate

1. Introduction

Liquid chromatography (LC) is the most flexible and one of the most powerful methods of separation of racemates. Microcrystalline cellulose triacetate (CTA) is widely used as a stationary phase for enantiomeric separations because it has some attractive properties, among them an often high enantioselectivity, a high loadability, a good mechanical stability, and a relatively low cost [1–3]. However, if this material is often used for preparative applications, it is rarely so for analytical separations because of the low efficiency of the swollen-CTA columns and because the cost advantage is minor in this latter case. So, despite its popularity in industry, limited information is available on the mechanisms involved in chromatographic enantioseparations with this phase, i.e., on these mechanisms that control retention, peak spreading and chiral recognition.

Recently, Seidel-Morgenstern and Guiochon [4,5] made a detailed study of the competitive adsorption of the two enantiomers of Tröger's base (TB) from

*Corresponding author. Address for correspondence: Department of Chemistry, University of Tennessee, 611 Buehler Hall, Knoxville, TN 37996-1600, USA. Tel.: +1-432-9740-733; fax: +1-423-9742-667.
E-mail address: guiochon@utk.edu (G. Guiochon)

0021-9673/99/$ – see front matter
PII: S0021-9673(99)00590-7

ethanol onto CTA and of the thermodynamic properties of this phase equilibrium. The single adsorption isotherm data measured for the two enantiomers, (−)- or *S*- and (+)- or *R*-TB, were well accounted for by the Langmuir isotherm and a quadratic isotherm, respectively. This result was valid in the temperature range between 30 and 50°C. The competitive isotherms were not measured, essentially because the poor column efficiency [110 and 170 theoretical plates for (+)- and (−)-TB, respectively] was too low to allow for accurate enough determinations using classical competitive frontal analysis. An attempt was made to model these isotherms using the ideal adsorbed solution theory. The result was only fair, as demonstrated by the moderate agreement between experimental and calculated elution profiles of the racemate. The enthalpies and isosteric heats of adsorption depend on both the temperature and the adsorbate concentration but to a different degree for the two enantiomers.

The mass transfer kinetics of TB in the phase system CTA–ethanol was studied under both linear and non-linear conditions [6–8]. It was found that the kinetic parameters representing the mass transfer rate, i.e., the apparent axial dispersion coefficient (D_a) in the equilibrium–dispersive model and the mass transfer rate coefficient (k_m) in the transport–dispersive model, depend on the TB concentration. A similar positive concentration dependence was also found for the lumped mass transfer rate coefficient ($k_{m,L}$) in the anion-exchange chromatography of bovine serum albumin (BSA) [9,10], and in the enantiomeric separation of D- and L-phenylalanine anilide on a polymeric imprinted stationary phase [11]. The same concentration dependence was also reported in studies of intraparticle diffusivity [12], tracer diffusivity [13], axial dispersion coefficient [14], effective diffusivity in bulk solutions [15], and mutual diffusion coefficient [16] of various compounds.

Band broadening in chromatography should be analyzed by considering axial dispersion and the three main mass transfer steps of the solute between the bulk mobile phase and the stationary phase. These steps are (1) the external mass transfer or transport of the solute molecules from the bulk mobile phase to the surface of the particles of stationary phase (fluid-to-particle mass transfer); (2) the diffusive transport through the pores of the stationary phase particles (intraparticle diffusion); and (3) the adsorption/desorption processes at the actual adsorption sites (adsorption/desorption kinetics) [17]. The presence of axial dispersion and the fluid-to-particle mass transfer resistance is inherent to all flow processes using a packed bed. The degree of axial dispersion observed depends on the skill in preparing an homogeneous packed column. The influence of the fluid-to-particle mass transfer on band spreading is usually small and well known.

By contrast, the characteristic features of intraparticle diffusion and the adsorption/desorption kinetics result from intrinsic properties of the packing materials which are related to its geometrical structure and are not yet completely understood. These intrinsic properties must be clarified in order to obtain a better understanding of the properties of CTA as a stationary phase. It might be predicted that the swollen structure of CTA influences intraparticle diffusion and that the contribution of the adsorption/desorption kinetics to band broadening is important compared to what it is with other phase systems of chromatography, e.g., in the reversed-phase and ion-exchange modes, because the chiral recognition actually takes place at the adsorption sites. In previous papers [18,19], we analyzed the concentration dependence of $k_{m,L}$ for BSA in anion-exchange chromatography and obtained information concerning the actual mass transfer kinetics in the four processes listed above. It was shown that surface diffusion influences the characteristics of the mass transfer of BSA and that the linear concentration dependence of $k_{m,L}$ resulted from the same dependence of the surface diffusion coefficient (D_s). The positive dependence of the coefficient D_s for BSA on its concentration could be interpreted by the heterogeneous surface model, suggesting the presence of a distribution of adsorption energy on the surface of the anion exchanger.

Although many papers have been published discussing enantiomeric separations on CTA, little information was obtained about the real features of the mass transfer kinetics in a CTA column. The goal of this work is to obtain new information on the mass transfer kinetics of *S*-TB in a CTA column and to provide an explanation for the positive concentration dependence of k_m. A quantitative analysis of

the thermodynamic properties of the mass transfer of *S*-TB in this phase system (CTA–ethanol) was also attempted.

2. Theory

There are various theories and models proposed for representing the phase equilibrium and the mass transfer kinetics in LC [17,20]. In this study, the adsorption equilibrium and the mass transfer kinetics of *S*-TB on CTA were expressed using the Langmuir isotherm and the lumped kinetic model, respectively. The details can be found in the original paper [7] and the relevant literature [17].

2.1. Adsorption equilibrium

The experimental data characterizing the adsorption equilibrium of *S*-TB on CTA were well accounted for by the simple Langmuir isotherm [4,5,7,8].

$$q = \frac{aC}{1 + bC} \tag{1}$$

where C and q are the concentration of *S*-TB in the mobile and the stationary phase, respectively, and a and b are numerical parameters independent of C.

2.2. Mass transfer kinetics

In this study, the concentration dependence of k_m was determined from the experimental breakthrough curves acquired in the frontal analysis. These curves were analyzed using the equations derived for local linear chromatography. It is assumed that, although the isotherm is not linear between $C=0$ and C, the breakthrough profile is that observed under imaginary linear conditions, at $C=C$, when a stream of concentration C is replaced by one of concentration $C+\Delta C$, at least if ΔC is sufficiently small.

2.2.1. The general kinetic model in chromatography

The general kinetic model of chromatography is a complete model which considers three phases in the column, (1) the bulk mobile phase percolating through the bed of particles; (2) the stagnant mobile phase which impregnates the porous particles; and (3) the stationary phase. The equation set of this model includes the mass balance equations of the analyte in the column and in the particles, and the kinetic equations describing the mass transfer between the three phases. From the first and the second moments of the solution of the general kinetic model, the height equivalent to a theoretical plate (HETP) (H) in linear chromatography is derived as follows [17].

$$H = \frac{2D_L}{u} + 2\left(\frac{k_1}{1+k_1}\right)^2 \times \left[\frac{ud_p}{6Fk_f} + \frac{ud_p^2}{60FD_e} + \left(\frac{k_p}{1+k_p}\right)^2 \frac{u}{Fk_{ads}}\right] \tag{2}$$

with

$$k_1 = F\left[\epsilon_p + (1-\epsilon_p)K_a\right] \tag{2a}$$

$$k_p = \frac{1-\epsilon_p}{\epsilon_p} K_a \tag{2b}$$

where D_L is the axial dispersion coefficient, u the average interstitial velocity of the mobile phase, d_p the particle diameter, F the phase ratio [$F=(1-\epsilon_T)/\epsilon_T$, with ϵ_T the total column porosity), k_f the external mass transfer coefficient, D_e the intraparticle diffusivity, k_{ads} the adsorption rate constant, ϵ_p the internal porosity of the particle, and K_a the adsorption equilibrium constant.

2.2.2. The lumped kinetic model in linear chromatography

When one of the contributions to the mass transfer kinetics dominates the other ones, the model of the chromatographic process can be simplified. It is often conveniently represented by the lumped kinetic model [17] which uses only one mass balance equation:

$$\frac{\partial C}{\partial t} + F\frac{\partial C_s}{\partial t} + u\frac{\partial C}{\partial z} = D_L\frac{\partial^2 C}{\partial z^2} \tag{3}$$

The transfer kinetics is then characterized by the simple mass transfer rate coefficient (k_m)

$$\frac{\partial C_s}{\partial t} = k_m(C_s^* - C_s) \tag{4}$$

where C_s is the concentration of the solute in the

stationary phase, C_s^* the solute concentration in the stationary phase when in equilibrium with a solution of concentration C [C_s^* is given by Eq. (1)], t the time, z the longitudinal distance along the column, and k_m the mass transfer rate coefficient. It is assumed in Eq. (4) that the driving force of the mass transfer is the difference between C_s^* and C_s and that the mass transfer rate is proportional to the driving force. Lapidus and Amundson [21] derived an analytical solution of the system of Eqs. (3) and (4) for a rectangular pulse and a linear isotherm. Recognizing that, in most cases of importance in chromatography, k_m is relatively large, van Deemter et al. [22] simplified this solution, showed that it was equivalent to a Gaussian profile and derived the following HETP equation

$$H = \frac{2D_L}{u} + 2\left(\frac{k_0'}{1+k_0'}\right)^2 \frac{u}{k_0' k_m} \quad (5)$$

where k_0' is the retention factor at infinite dilution, proportional to the equilibrium constant and the coefficient a of the isotherm [Eq. (1)]. The comparison of Eqs. (2) and (5) gives

$$\frac{F}{k_0' k_m} = \frac{d_p}{6k_f} + \frac{d_p^2}{60D_e} + \left(\frac{k_p}{1+k_p}\right)^2 \frac{1}{k_{ads}} \quad (6)$$

Eq. (6) indicates that the mass transfer coefficient in the solid film linear driving force model (k_m) is related to the three kinetic parameters, the external mass transfer coefficient (k_f), the intraparticle diffusivity (D_e), and the adsorption rate constant (k_{ads}), and that the contributions to band broadening due to these three mass transfer processes are additive.

2.2.3. A HETP equation in local linear chromatography

Similar to Eq. (5), the following HETP equation was derived for nonlinear chromatography, from the shock layer theory in frontal analysis, under constant pattern behavior

$$H = \frac{2D_L}{u} + 2\left(\frac{K}{1+K}\right)^2 \frac{u}{K k_m} \quad (7)$$

where K is the slope of the isotherm chord [$K = FK_a = F(\Delta q/\Delta C)$]. Eq. (7) is similar to Eq. (5) where k_0' is replaced by K, which makes this equation valid under nonlinear conditions. Eq. (7) is valid as long as the column efficiency is not very low [17]. It indicates that the contributions of the axial dispersion and of the other mass transfer processes are additive in nonlinear chromatography like in linear chromatography, at least in frontal analysis, assuming the solid film linear driving force model. The contributions of each mass transfer process in nonlinear frontal analysis, i.e., (1) the fluid-to-particle mass transfer, (2) the intraparticle diffusion, and (3) the adsorption/desorption are lumped into only one kinetic parameter, k_m, which is a considerable simplification.

In this study, the breakthrough curves were measured under local linear isotherm conditions (described later). Similar to Eq. (6), valid in the case of linear chromatography, the following equation can be derived for local linear chromatography.

$$\frac{F}{K k_m} = \frac{d_p}{6k_f} + \frac{d_p^2}{60D_e} + \left(\frac{k_p}{1+k_p}\right)^2 \frac{1}{k_{ads}} \quad (8)$$

Eq. (8) represents the correlation between k_m and the different mass transfer kinetic parameters, i.e., k_f, D_e, and k_{ads}. In this study, it was assumed on the basis of the parallel diffusion model that the intraparticle diffusion consists of the pore and the surface diffusions [23,24], so we have

$$D_e = D_p + (1-\epsilon_p) K_a D_s \quad (9)$$

where D_p and D_s are the pore diffusivity and the surface diffusion coefficient, respectively. Eq. (9) was frequently used in studies on the intraparticle mass transfer in linear and local linear isotherm systems previously published. The following equation was used for correlating D_p with the molecular diffusivity (D_m) [17].

$$D_p = \left(\frac{\epsilon_p}{2-\epsilon_p}\right)^2 D_m \quad (10)$$

3. Experimental

In this study, an attempt was made to further advance the quantitative analysis of the mass transfer kinetics of *S*-TB on CTA by reevaluating the experimental data [7], using recent theoretical results in the theory of mass transfer in chromatography [17]. The experimental results on the phase equilibrium

and the mass transfer kinetics were determined from the breakthrough curves measured in the mode of local linear frontal analysis. Only the simple, limited information on the experimental conditions that is presented below is necessary for understanding the new results presented in this study. Ample details on the experimental work can be found in an original paper [7].

Microcrystalline CTA (particle diameter, 15–35 μm) was packed in a stainless steel column (25× 0.46 cm), using a slurry method. The hold-up volume (V_0) was determined to be 2.517 ml from the elution volume of an unretained solute (1,3,5-tri-*tert*.-butylbenzene, TTBB) [25]. The total porosity (ϵ_T) and the phase ratio (F) of the CTA column were calculated as 0.606 and 0.650, respectively. The number of theoretical plates (N) was 550 for TTBB. The frontal analysis experiments were made at 40°C, with pure ethanol as the mobile phase. The breakthrough curves were measured in a range of mobile phase flow-rate between 0.2 and 1.2 ml min^{-1}. The range of the concentration steps for the measurement of the breakthrough curves was 0.3 or 0.4 mg ml^{-1}. Each breakthrough curve gave one data point of the equilibrium isotherm. The data of the phase equilibrium were fitted to the Langmuir isotherm [Eq. (1)]. The dependence of the experimental HETP on the mobile phase flow velocity was represented by a modified van Deemter equation (described later). The parameters of the mass transfer kinetics were determined from the slope and the intercept of the linear relation between H and u.

4. Results and discussion

In order to clarify the characteristic features of the mass transfer kinetics of *S*-TB in the CTA column, some kinetic parameters concerning the different mass transfer processes in the CTA column were first calculated. These parameters were derived from an analysis of the previous experimental results on the phase equilibrium and the mass transfer rate of *S*-TB determined from the breakthrough curves in single step frontal analysis [7]. The individual contributions to band broadening of each of the mass transfer processes taking place in the column or in the CTA particles were individually evaluated and compared with each other. Then, an attempt was made to explain the dependence of k_m on the concentration of *S*-TB by considering the concentration dependence of the phase equilibrium. Finally, a quantitative interpretation of the thermodynamic properties of the mass transfer of *S*-TB in the CTA column was provided.

4.1. Adsorption equilibrium

Fig. 1 summarizes the experimental isotherm data of *S*-TB in the phase system made of CTA and ethanol. These data are well accounted for by the Langmuir isotherm [Eq. (1)] [4,5,7,8]. The degree of curvature of the equilibrium isotherm is not important. The values of the numerical parameters of the Langmuir isotherm, i.e., a and b, were determined to be 3.139 and 0.116, respectively [7]. The saturation capacity ($q_s = a/b$) was 27.1 mg ml^{-1}. In this study, the concentration of *S*-TB was increased up to 3.0 mg ml^{-1}, at which concentration q was ca. 7 mg ml^{-1}. So, the maximum value of the product bC was 0.35 and the maximum surface coverage ($\theta = q/q_s$) was 0.25 q_s. Fig. 1 illustrates these results.

As described above, the concentration step for the measurement of the breakthrough curves was between 0.3 and 0.4 mg ml^{-1} [7]. Because the degree of curvature of the equilibrium isotherm is relatively small, it was expected that the experimental data on the mass transfer kinetics could be derived from these breakthrough curves by assuming that the isotherm was locally linear. Fig. 2 illustrates the values of $\Delta q/\Delta C$ (solid line) and dq/dC (dotted line) as a function of C. When $\Delta q/\Delta C$ was calculated, ΔC was taken as 0.4. For the Langmuir isotherm, dq/dC was calculated as

$$\frac{dq}{dC} = \frac{a}{(1 + bC)^2} \tag{11}$$

As illustrated in Fig. 2, the solid and the dotted lines are exactly overlaid, indicating that the frontal analysis experiments were truly made under conditions of locally linear equilibrium.

4.2. Mass transfer rate coefficient

The experimental breakthrough curves were fitted

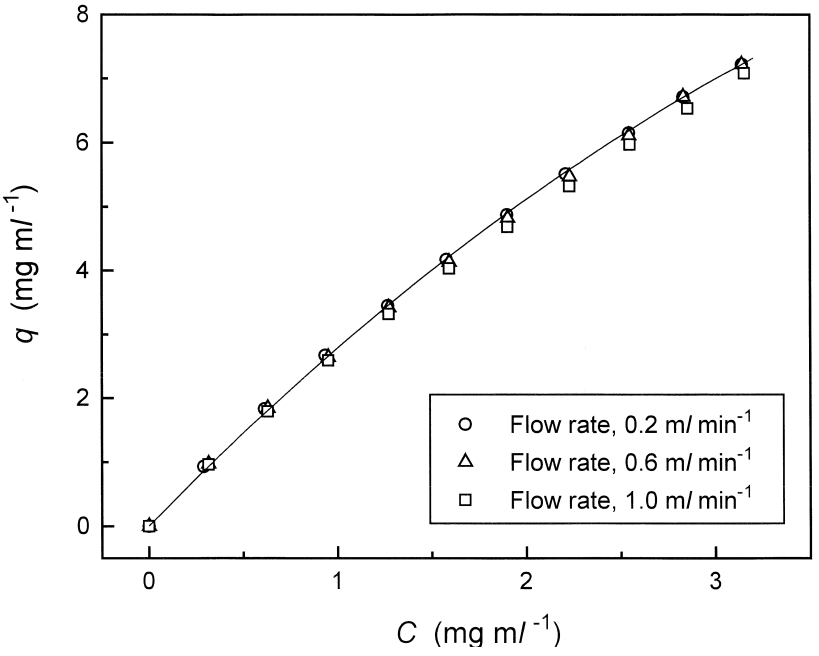

Fig. 1. Equilibrium isotherm of *S*-TB on CTA.

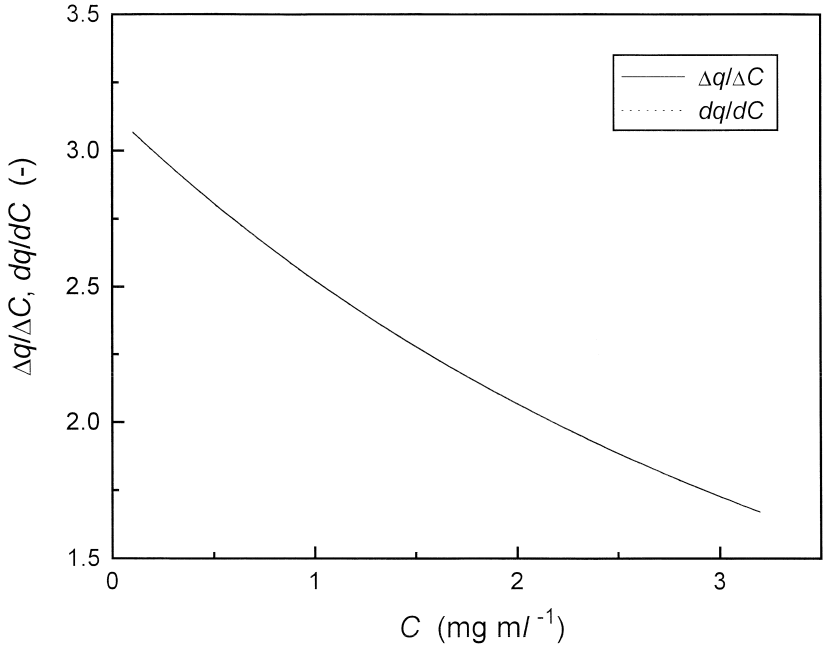

Fig. 2. Comparison between the slope of the isotherm chord ($\Delta q/\Delta C$) and the tangent of the equilibrium isotherm (dq/dC). The solid and dotted lines are almost completely superimposed, indicating that the assumption of local linear isotherm behavior made in this study is valid.

to both the equilibrium-dispersive model and the transport model in order to obtain the mass transfer rate coefficient [7]. The parameter for which the best agreement was observed between experimental and calculated breakthrough curves was taken as the best value of the apparent Peclet number (Pe) in the equilibrium-dispersive model and the best value of the apparent Stanton number (St) in the transport model. The definitions of these two parameters are as follows.

$$\mathrm{Pe} = \frac{uL}{D_a} \tag{12}$$

$$\mathrm{St} = \frac{k_{m,L}L}{u} \tag{13}$$

where D_a is the apparent axial dispersion coefficient, into which all contributions to band broadening originating in the column are lumped together, and $k_{m,L}$ is the lumped mass transfer rate coefficient representing the contributions of axial dispersion, the fluid-to-particle mass transfer, intraparticle diffusion, and adsorption/desorption kinetics to band broadening. The HETP is described by using the corresponding two nondimensional parameters defined as follows

$$H_{Pe} = \frac{2L}{\mathrm{Pe}} \tag{14}$$

$$H_{St} = \frac{K}{(1+K)^2}\frac{2L}{\mathrm{St}} \tag{15}$$

Under locally linear isotherm conditions, the following modified van Deemter equation can be derived from Eq. (7).

$$H = A + C_s' u \tag{16}$$

where:

$$C_s' = \frac{2K}{(1+K)^2 k_m} \tag{17}$$

The two terms in the right-hand-side (RHS) of Eq. (16) account for the respective contributions of axial dispersion and the mass transfer resistance to band broadening. Eq. (16) does not include the conventional B term that accounts for axial molecular dispersion. This omission is justified in the present experimental case because the mass transfer resistance is unusually high and this third term would be negligible compared to the other two terms [7]. The two parameters in Eq. (16), A and C_s', were respectively determined from the intercept and the slope of the linear plot between H_{Pe} or H_{St} and u [7]. The values of k_m were calculated from those of C_s' thus obtained, using Eq. (17). Table 1 lists the resultant values of A, C_s', and k_m. Fig. 3 shows that k_m increases with increasing concentration of *S*-TB, and that the rate of this increase remains moderate. When C increases 20-fold, from 0.15 to 3.0 mg ml^{-1}, k_m increases only by a factor of about 1.6.

Similarly, from the strong dependence of the column efficiency on the temperature and the mobile-phase flow-rate, Isaksson et al. [26] considered that the slow mass transfer kinetics was the largest contribution to band broadening in the CTA column. Rizzi [27] also investigated the peak broadening process on swollen CTA particles and reported that the most important contribution to the plate height arose from the slow mass transfer in the column. The characteristic features of the mass transfer kinetics inside swollen CTA particles (the slow intraparticle diffusion and the slow adsorption/desorption kinetics) should be analyzed in more detail for a better understanding of the performance of CTA as a stationary phase for the enantiomeric separation of *S*-TB.

4.3. Estimation of the adsorption rate constant

Eq. (9) suggests that D_e increases with increasing K when the contribution of the surface diffusion to the intraparticle diffusion cannot be completely neglected compared with that of the pore diffusion.

Table 1
Parameters of the mass transfer kinetics

Concentration (mg ml^{-1})	A (cm)	C_s' (s)	k_m (s^{-1})
0.15 (0.0–0.3)[a]	0.1945	$1.00\cdot10^{-3}$	0.124
0.15 (0.0–0.3)	0.1617	$7.28\cdot10^{-4}$	0.111
1.45 (1.3–1.6)	0.1740	$9.43\cdot10^{-4}$	0.141
1.45 (1.3–1.6)	0.1727	$8.97\cdot10^{-4}$	0.149
3.0 (2.8–3.2)	0.1860	$7.78\cdot10^{-4}$	0.177
3.0 (2.8–3.2)	0.1843	$1.12\cdot10^{-3}$	0.190

[a] The numbers in parentheses represent the ranges of the concentration steps of the breakthrough curves in the frontal analyses.

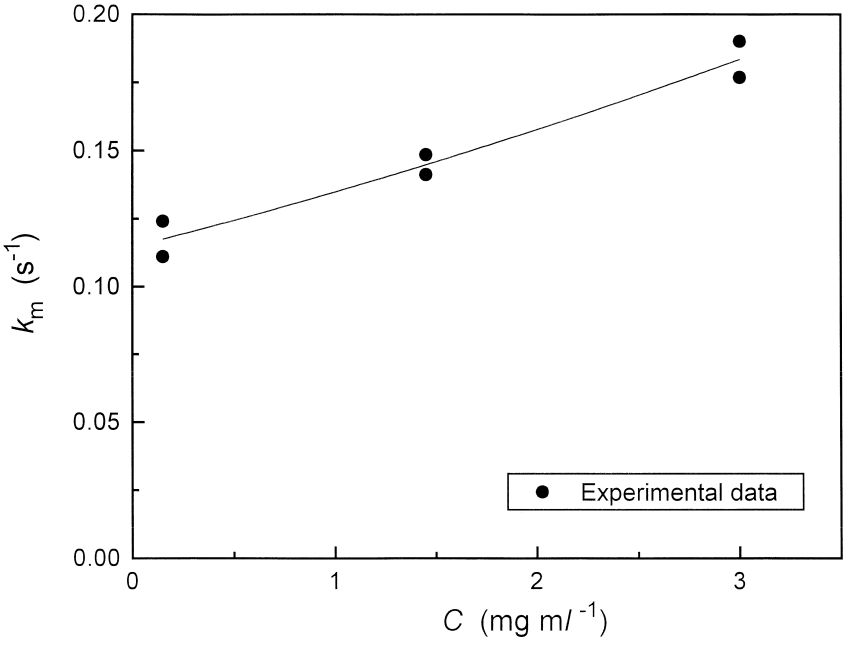

Fig. 3. Dependence of k_m on the concentration of *S*-TB.

At $K=\infty$, $F/(Kk_m)$ in Eq. (8) would be equal to the sum of two terms, i.e., $(d_p/6k_f)+(1/k_{ads})$, because the value of $[k_p/(1+k_p)]^2$ is then unity and the second term in the RHS of Eq. (8) might be neglected. Fig. 4 illustrates the plot of $F/(Kk_m)$ against $1/K$. The dotted line represents the result of the first-order regression of the experimental data, the solid line that of the second-order regression. Both the third- and fourth-order regressions gave the same correlation as the second-order regression.

From the intercept of the second-order regression in Fig. 4, the sum $(d_p/6k_f)+(1/k_{ads})$ is found to be 1.82. The value of the intercept of the linear regression in Fig. 4 is 2.38. The change in K is accompanied with the individual variations in the contributions of each term in Eq. (8) including D_e or k_p. As a consequence, $F/(Kk_m)$ changes. However, it is not clear which function can most sufficiently represent the variation in $F/(Kk_m)$ due to the change in K. The manner of the change in $F/(Kk_m)$ depends on the values of the kinetic parameters in Eq. (8) and the experimental conditions. Furthermore, experimental data cannot be acquired at sufficiently low values of $1/K$ because the rise of the equilibrium isotherm at low concentrations is not very steep as shown in Fig. 1. Although it is more likely that the intercept is between 1.82 and 2.38, the result derived from the higher order regression was used in this study.

The value of k_{ads} was estimated by subtracting the contribution of $d_p/(6k_f)$ from the value of the intercept. In this study, k_{ads} was assumed to be independent of C. The value of k_f was estimated using the Wilson–Geankopolis equation [28]

$$\mathrm{Sh} \equiv \frac{k_f d_p}{D_m} = \frac{1.09}{\epsilon}\mathrm{Sc}^{1/3}\mathrm{Re}^{1/3} \quad (0.0016 < \mathrm{Re} < 55) \qquad (18)$$

The molecular diffusivity (D_m) of *S*-TB was derived from the Wilke–Chang equation [17,29,30].

$$D_{m,s} = 7.4 \cdot 10^{-8}\frac{(\alpha_{A,sv}M_{sv})^{1/2}T}{\eta_{sv}V_{b,s}^{0.6}} \qquad (19)$$

where the subscripts s and sv denote *S*-TB and the solvent, respectively, α_A the association coefficient, M the molecular mass, η the viscosity, T the

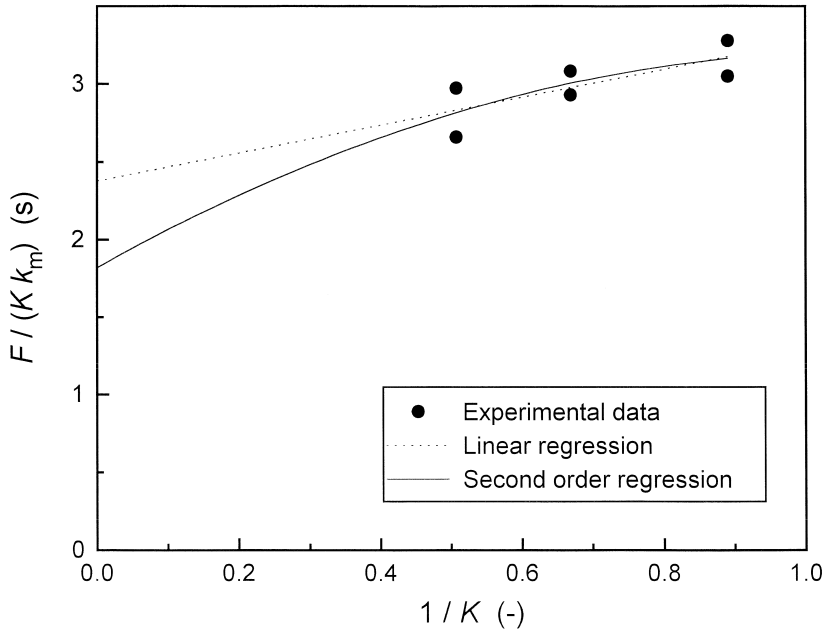

Fig. 4. Correlation between $F/(Kk_m)$ with $1/K$ for the estimation of k_{ads}.

absolute temperature, and V_b the molar volume at the normal boiling point. At a flow-rate of 0.7 ml min^{-1} (the intermediate value of the flow-rate range investigated), the value of $d_p/(6k_f)$ for *S*-TB was calculated to be $1.9 \cdot 10^{-2}$ s, which is two-orders of magnitude smaller than the intercept, suggesting that, in this case, the contribution of the fluid-to-particle mass transfer to band broadening is negligibly small. In this analysis, the dependence of k_f on the *S*-TB concentration was not considered. This assumption has little influence on the result because of the small contribution of the fluid-to-particle mass transfer to peak spreading. The value of k_{ads} was calculated as 0.56 s^{-1} from the intercept of the second-order regression of the experimental data, i.e., 1.82. On the other hand, the value of k_{ads} would be 0.42 s^{-1} if the intercept of the linear regression, i.e., 2.38, were used. Both values of k_{ads} are not only of the same order of magnitude; they are very close.

4.4. Comparison of the individual contributions of the four mass transfer processes to the HETP

The following HETP equation is derived from Eqs. (7) and (8).

$$H_{total} = \frac{2D_L}{u} + 2\left(\frac{K}{1+K}\right)^2 \times \left[\frac{ud_p}{6Fk_f} + \frac{ud_p^2}{60FD_e} + \left(\frac{k_p}{1+k_p}\right)^2 \frac{u}{Fk_{ads}}\right] \quad (20)$$

$$H_{total} = H_{ax} + H_f + H_d + H_r \quad (20a)$$

Eq. (20) has a form similar to Eq. (2) and correlates the total HETP (H_{total}) with the different kinetic parameters. As described earlier, the value of H_{ax} was obtained from the intercept of the linear plot of H_{Pe} or H_{St} versus u. Both H_f and H_r can be calculated from k_f which, in turn, is reasonably estimated through Eq. (18) and from k_{ads} obtained in the previous section. The values of D_e and H_d can also be derived from Eq. (8) because the contributions of the two mass transfer processes other than intraparticle diffusion could also be estimated. Accordingly, the contributions of the four terms in the RHS of Eq. (20a) to H_{total} can be calculated and compared with each other. Fig. 5a and 5b show the dependence of H_{total} and of each of the four contri-

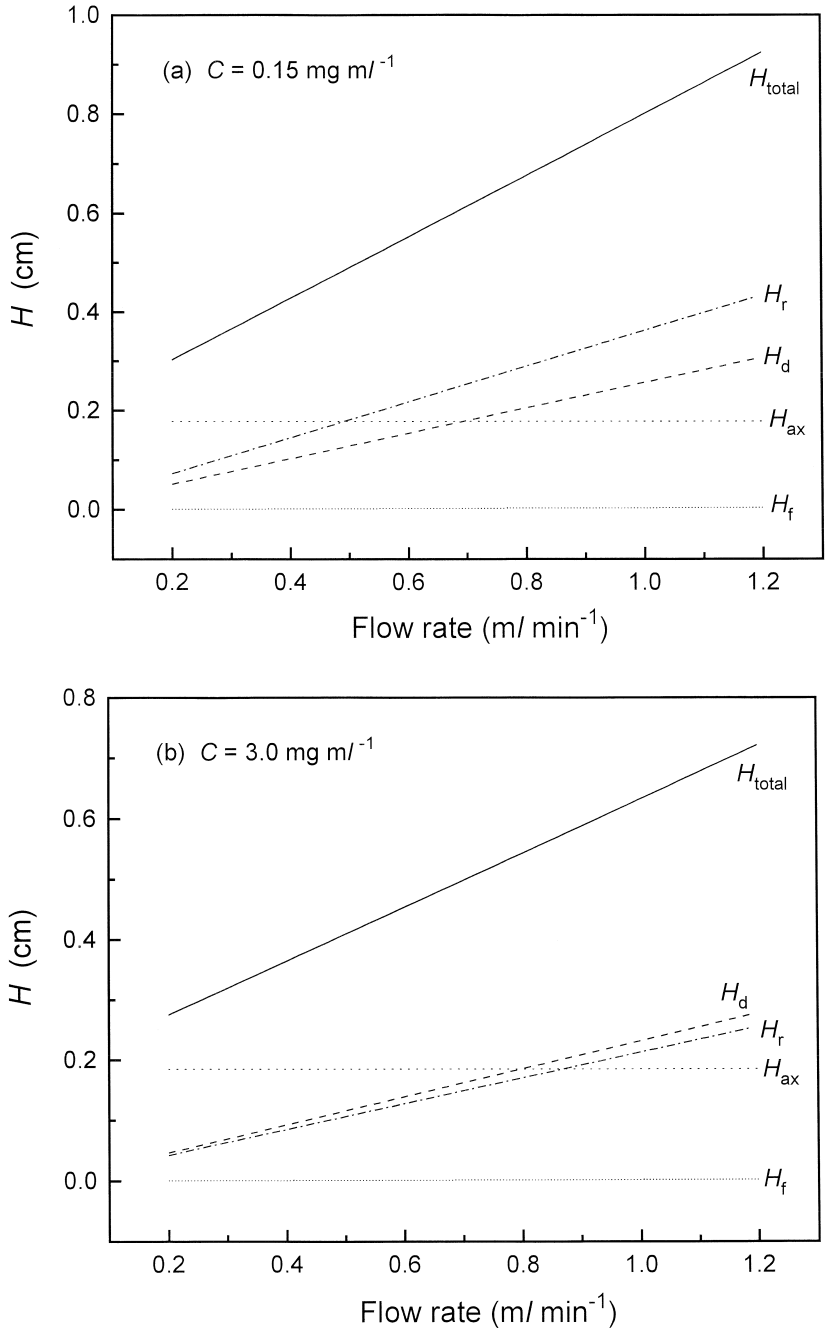

Fig. 5. Comparison of the contribution of the mass transfer resistance at each kinetic process in the column to the overall efficiency at different flow-rates of the mobile phase. HETP: H_{total}, the overall column efficiency; H_{ax}, the contribution of the axial dispersion; H_f, the contribution of the fluid-to-particle mass transfer; H_d, the contribution of the intraparticle diffusion; H_r, the contribution of the adsorption/desorption. (a) $C=0.15$ mg ml^{-1}, (b) $C=3.0$ mg ml^{-1}.

butions on the mobile phase flow-rate at two different concentrations of *S*-TB, i.e., $C=0.15$ and 3.0 mg ml^{-1}.

It is usually assumed that axial dispersion is the combined result of two different mechanisms, molecular diffusion and fluid or Eddy diffusion. As indicated in Eq. (16), however, the contribution of molecular diffusion (the *B* term) is negligible in this study. At low concentrations of *S*-TB (Fig. 5a), the contribution H_{ax}, which is constant, irrespective of the flow-rate, is the largest contribution to H_{total} at low flow-rates. The contributions H_d and H_r increase with increasing flow-rate and dominate at high flow-rates. The contribution H_r is larger than H_d. The contribution H_f is always negligibly small. In Fig. 5b, a similar situation is observed. The contribution of H_d to H_{total} is almost the same as or even larger than that of H_r. Fig. 5a and 5b show that intraparticle diffusion also plays an important role in band broadening at high flow-rates.

4.5. Information about the intraparticle diffusion

4.5.1. Estimation of pore diffusivity

Eq. (9) suggests that D_e approaches D_p as the equilibrium constant, K_a, tends toward zero. Fig. 6 shows the plot of D_e against *K*. From its intercept, D_p was estimated as $4.9\cdot10^{-8}$ cm^2 s^{-1}. Compared with D_m of *S*-TB at 40°C, estimated by Eq. (19), i.e., $8.0\cdot10^{-6}$ cm^2 s^{-1}, D_p is smaller than D_m by a factor of approximately 160. Experimental results confirmed that D_p is usually between three- and 30-times smaller than D_m for typical chromatography packing materials [17]. The ratio D_p/D_m estimated in this study is smaller than the previous observation. From the value of D_p determined from Fig. 6 and that of D_m estimated by the Wilke–Chang equation, a value of ϵ_p of 0.15 was calculated from Eq. (10) for the enantioseparation system using CTA and ethanol. Although this is relatively small compared with the ordinary values of ϵ_p previously reported for other

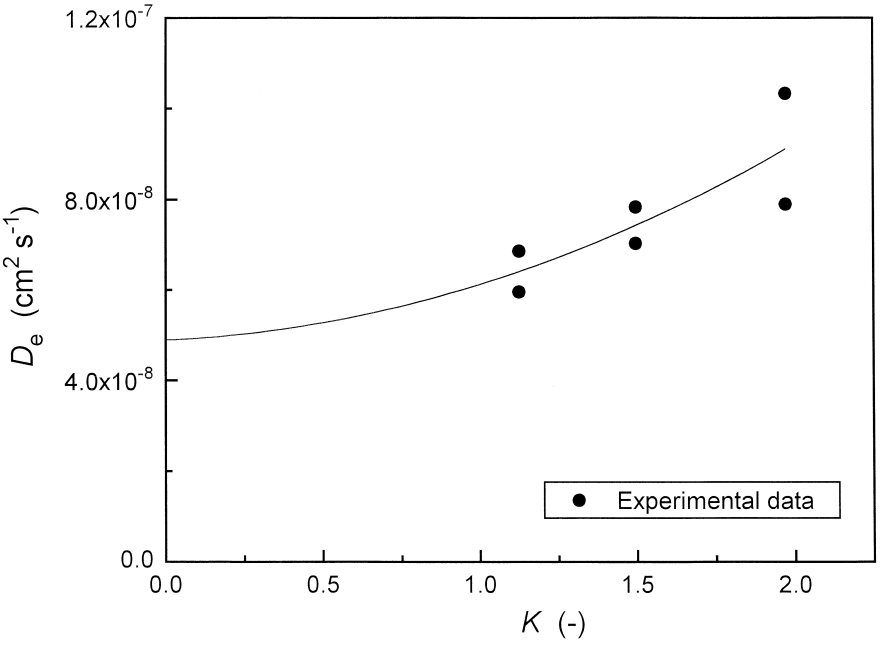

Fig. 6. Correlation between D_e with *K* for the estimation of D_p. The solid line represents the second-order regression of the experimental data and provides $D_p=4.9\cdot10^{-8}$ cm^2 s^{-1}. Similarly, the third- and fourth-order regressions give $D_p=5.4\cdot10^{-8}$ and $3.1\cdot10^{-8}$ cm^2 s^{-1}, respectively. A linear regression was not made because D_s could not be assumed to be constant. These three values of D_p are close. It is unlikely that the conclusions of this study are seriously influenced by the uncertainty of the value of D_p.

porous materials, similarly small values of ϵ_p have also been reported as the porosities of bidispersed activated carbons and other adsorbents [24]. Note also that the column efficiency is abnormally low for the TB enantiomers: the column efficiency exceeded 5000 theoretical plates for water [4] and was 550 plates for tri-*tert*.-butylbenzene [7] but it was only of the order of 100 plates for *S*-TB [4,7]. Such a low efficiency could be explained by a low value of D_p.

The value of ϵ_p reflects the small D_p. This small ratio D_p/D_m is probably due to the influence of the physical properties of the micropores of CTA on pore diffusion. Although it is well known that the CTA particles swell in ethanol, the influence of the swelling on the physical and chemical properties of this material is still unclear. It is likely that the *S*-TB molecules may migrate through CTA in the manner of pore diffusion across the network of micropores filled with a mixture of the mobile phase, ethanol, and some stationary phase components, i.e., glucose chains. Some properties, for example, the structure of the micropores and the viscosity of ethanol, may be affected by the presence of ethanol in the crystalline structure of CTA or by the dissolution of some CTA components into ethanol. It is also likely that the entire porosity of CTA available to ethanol molecules is not available to larger *S*-TB molecules. The mass transfer rate of solutes inside swollen CTA particles seems to be influenced by the swelling conditions of CTA.

Isaksson et al. [26] reported some data on the physical and chemical properties of CTA and unmodified native cellulose. The values of the total pore volume (V_p) and the surface area (S_A) of CTA were determined by the nitrogen BET method as 0.09 $cm^3\ g^{-1}$ and 6.1 $m^2\ g^{-1}$, respectively. Those of the unmodified native cellulose were respectively 0.04 $cm^3\ g^{-1}$ and 1.1 $m^2\ g^{-1}$. The average pore radius (r_p) of dry CTA is estimated as about 30 nm ($=2V_p/S_A$) by assuming a cylindrical pore structure. Although the real pore shape of CTA is probably not cylindrical, the size of the pores of CTA seems to be roughly estimated. Isaksson et al. [26] cited the information about the micropores of microcrystalline cellulose (not CTA) provided by the BET method and a water vapor method. The surface area of microcrystalline cellulose was respectively determined as 1.0 and 150 $m^2\ g^{-1}$ by the BET and water vapor methods. The much higher value obtained by the water vapor method was attributed to the swelling of cellulose. It is quite possible, however, that nitrogen could not penetrate between the cellulose fibers at the low temperature used in the BET measurements while water vapor had access at a higher temperature.

Isaksson et al. [26] also reported information on the swelling of CTA in various solvents. A swelling factor (S_F) was defined as $S_F=$(volume of swollen CTA/volume of non-swollen CTA)-1. In many solvents, except water, the value of S_F measured was about 40%. In water, S_F was 5%. If CTA and microcrystalline cellulose have the same degree of swelling, the surface area of CTA should increase considerably by swelling. If we assume that the pore volume of CTA increases by 5% and that the surface area of CTA in water is 150 $m^2\ g^{-1}$, the pore radius should be 1.3 nm. On the other hand, the Stokes radius (r_A) of *S*-TB is related to the diffusivity by the Stokes–Einstein equation. Because the molecular diffusivity of *S*-TB in ethanol is estimated as $8\cdot10^{-6}$ $cm^2\ s^{-1}$ at 40°C by the Wilke–Chang equation, r_A is calculated as 0.34 nm. While the size of the pores of dry CTA is about two-orders of magnitude larger than the *S*-TB molecule, the difference between r_p and r_A is not so large under swollen conditions, even in water. Although a distinct conclusion cannot be obtained, these hypothetical calculations imply the possibility of the influence of the intrinsic pore properties of swollen CTA on the hindered intraparticle diffusion of *S*-TB in CTA. Rizzi [31] investigated peak dispersion in swollen CTA columns by changing the mobile phase composition, and pointed out the influence of changes in the solvent viscosity, in the three-dimensional structure of CTA, and in the availability and accessibility of the adsorption sites on the peak dispersion. Definitive conclusions have not yet been derived for the mechanisms and properties of mass-transfer phenomena inside swollen CTA particles.

Frey et al. [32] related D_e to D_m by assuming the following equation.

$$D_e = \frac{D_m \lambda}{\tau} \tag{21}$$

where τ and λ are the tortuosity factor and the hindrance parameter, respectively. The value of λ

depends on several factors, such as the molecular volume of the solute, the size and structure of the pores, and the viscosity of the solvent filling the pores. Park et al. [33] studied the diffusion of BSA labeled with *p*-(isothiocyanato)azobenzene in polyacrylamide (PA) gel by means of holographic relaxation methods. They reported that the ratio of the diffusivity of the probe in the gel to that in the pure solvent decreased with increasing PA concentration and that the negative concentration dependence of the ratio D_p/D_m was represented by a stretched exponential function. They obtained relatively small values of D_p/D_m, close to 1/100. Although kinetic data on intraparticle diffusion are usually analyzed by taking λ as unity, λ might be smaller than unity under the experimental conditions of this study because of some of the reasons given above. However, more detailed studies are necessary to reach definite conclusions regarding intraparticle diffusion of solutes in this phase system. For this purpose, the actual characteristics of the mass transfer processes inside CTA particles must be studied individually.

Fig. 7 shows a plot of D_e versus C. D_e decreases with increasing *S*-TB concentration. Fig. 7 also illustrates the contributions of pore and surface diffusions to intraparticle diffusion. In this study, the concentration of *S*-TB was increased up to 3 mg ml^{-1} (0.3%). The concentration dependence of D_m was not taken into account because experimental results suggested that the concentration dependence of D_m was small in the concentration range 0–5% [17]. Because D_p was derived from Eq. (10), D_p is also assumed to be independent of C. The difference between D_e (shown in solid circles) and D_p (open circles) corresponds to the contribution of surface diffusion (open triangles). While the contributions of pore and surface diffusions to intraparticle diffusion are comparable in the low concentration range, the role of pore diffusion is predominant at high concentrations.

4.5.2. Estimation of surface diffusion coefficient

The value of D_s was estimated from k_m by using the other kinetic parameters in Eqs. (8) and (9), i.e., k_f, D_p, and k_{ads}. It is of the order of $1 \cdot 10^{-8}$ cm^2 s^{-1}. Although D_s depends on the combination of solute, stationary and mobile phases in the separation system, it is relevant to refer to data on D_s available in the literature. Miyabe and Guiochon [34] reviewed

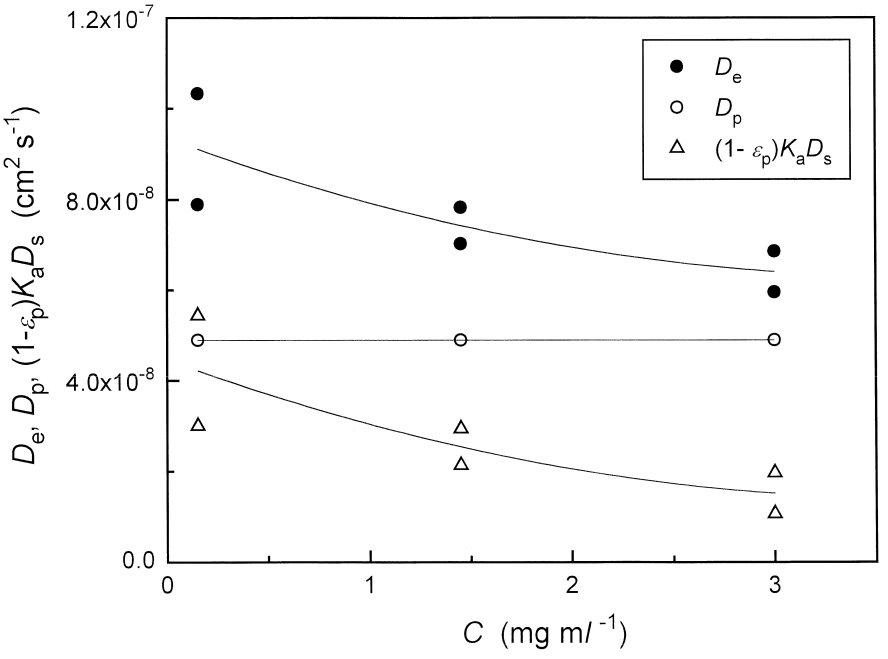

Fig. 7. Comparison of the contribution of the pore and the surface diffusions to the intraparticle diffusion.

surface diffusion data determined in reversed-phase liquid chromatography (RPLC) and reported that D_s was usually between $1\cdot10^{-7}$ and $1\cdot10^{-5}$ cm^2 s^{-1} under common RPLC conditions. There are other experimental data on surface and lateral diffusion in RPLC. Bogar et al. [35] determined the lateral diffusion coefficient of pyrene as $2.5\cdot10^{-7}$ cm^2 s^{-1} in a system consisting of a C_{18} packing material and a methanol–water mixture (75:25, v/v). Wong and Harris [36] reported D_s for iodine on a methyl-silica surface in contact with methanol–water solutions (75:25 and 50:50, v/v) as $7.2\cdot10^{-8}$ and $3.9\cdot10^{-8}$ cm^2 s^{-1}, respectively. Zulli et al. [37] measured the lateral diffusion coefficient of acridine orange at the water–C_{18} interface and reported $D_s=1.3\cdot10^{-7}$ cm^2 s^{-1}. Hansen and Harris [38] measured D_s for rubrene on a C_{18} bonded phase and reported values of $1.5\cdot10^{-9}$, $2.1\cdot10^{-9}$, and $2.8\cdot10^{-9}$ cm^2 s^{-1} for 0, 10, and 20% methanol in aqueous solutions, respectively. The results in these publications suggest D_s to be a few orders of magnitude smaller than the molecular diffusivity in the bulk solution and to increase with increasing concentration of the organic modifier (e.g., methanol and acetonitrile) in the aqueous mobile phase. A few experimental data have also been presented on the surface diffusion of macromolecules. Tilton et al. [39] measured the lateral mobility of eosin isothiocyanate-labeled BSA on two different adsorbents, poly(methylmethacrylate) and poly(dimethylsiloxane), and reported values of $1.2\cdot10^{-9}$ cm^2 s^{-1} for the former and $2.6\cdot10^{-9}$ cm^2 s^{-1} for the latter. Yoshida et al. [40] reported D_s of BSA on chitosan particles as $4.7\cdot10^{-10}$ cm^2 s^{-1} and $2.4\cdot10^{-9}$ cm^2 s^{-1} at infinite dilution, with ratios D_s/D_m of 1/1460 and 1/290, respectively, D_m being estimated at $6.8\cdot10^{-7}$ cm^2 s^{-1}. The values of D_s in Fig. 8 and the ratio D_s/D_m (ca. 1/500 in this study) are comparable with these data, suggesting that appropriate values of D_s were probably obtained.

Fig. 8 illustrates the correlation between D_s and the concentration of *S*-TB. Although the data are somewhat scattered, it seems that the concentration dependence of D_s is weak. While C increases 20-fold (from 0.15 to 3.0 mg ml^{-1}), D_s decreases by only 60%. In previous papers [18,19,34], we demonstrated that surface diffusion has a significant influence on the mass transfer kinetics in chromatography and that D_s increases with increasing solute concentration in the phase systems of both RPLC and anion-exchange chromatography. In RPLC on C_{18}-silica [34], the

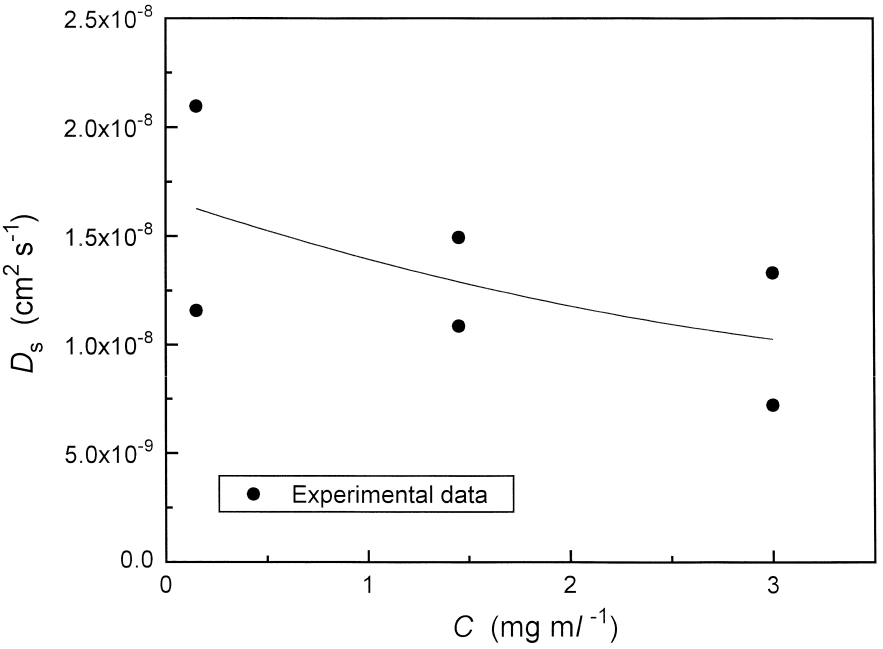

Fig. 8. Concentration dependence of D_s of *S*-TB.

dependence of D_s for *p-tert.*-octylphenol on its concentration was interpreted with the chemical potential driving force model. In anion-exchange chromatography [18,19], the heterogeneous surface model could represent the positive dependence of D_s on the concentration of BSA. The characteristics of mass-transfer in the CTA particles differ probably from those observed in other phase systems. The acquisition and analysis of further experimental data concerning the mass-transfer kinetics in this system are required to derive general conclusions.

4.6. Explanation of the positive concentration dependence of k_m

The rate coefficient k_m increases with increasing concentration of *S*-TB (Fig. 3). An attempt was made to interpret this dependence. As shown in Eq. (8), k_m accounts for the contributions of the three mass transfer processes in the CTA column. The following equation is easily derived from Eq. (8).

$$\frac{1}{k_m} = \frac{Kd_p}{6Fk_f} + \frac{Kd_p^2}{60FD_e} + \left(\frac{k_p}{1+k_p}\right)^2 \frac{K}{Fk_{ads}} \quad (22)$$

or:

$$\delta_{total} = \delta_f + \delta_d + \delta_r \quad (22a)$$

where δ_{total}, δ_f, δ_d, and δ_r denote the reciprocal of k_m, and the first, second, and third term of the RHS of Eq. (22), respectively. Fig. 9 illustrates the dependence of each of these contributions on the *S*-TB concentration. The contribution of the fluid-to-particle mass transfer (δ_f) is negligible. The mass transfer resistances due to both the intraparticle diffusion (δ_d) and the adsorption/desorption kinetics (δ_r) are nearly identical. However, the profile of δ_r resembles that of δ_{total} ($=1/k_m$), while δ_d exhibits a slow, linear decrease. It is probable that the concentration dependence of k_m results mainly from that of the kinetics of adsorption/desorption.

As explained earlier, we assumed in this study k_{ads} to be independent of the concentration of *S*-TB. In Fig. 10, the reciprocal of the coefficient of the third

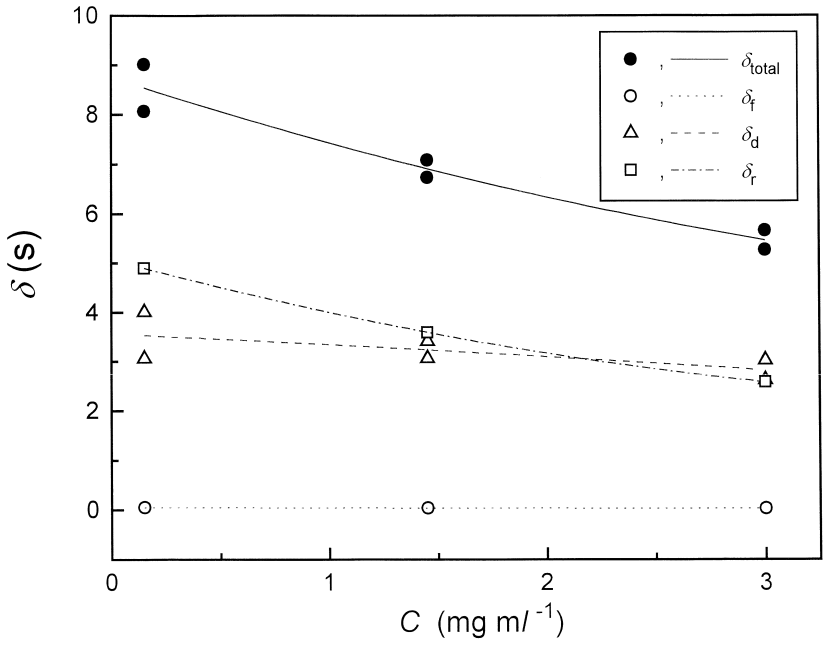

Fig. 9. Comparison of the contribution of each kinetic process to the mass transfer resistance in the column at different *S*-TB concentrations. Mass transfer resistance: δ_{total}, the overall resistance in the column; δ_f, the contribution of the fluid-to-particle mass transfer; δ_d, the contribution of the intraparticle diffusion; δ_r, the contribution of the adsorption/desorption.

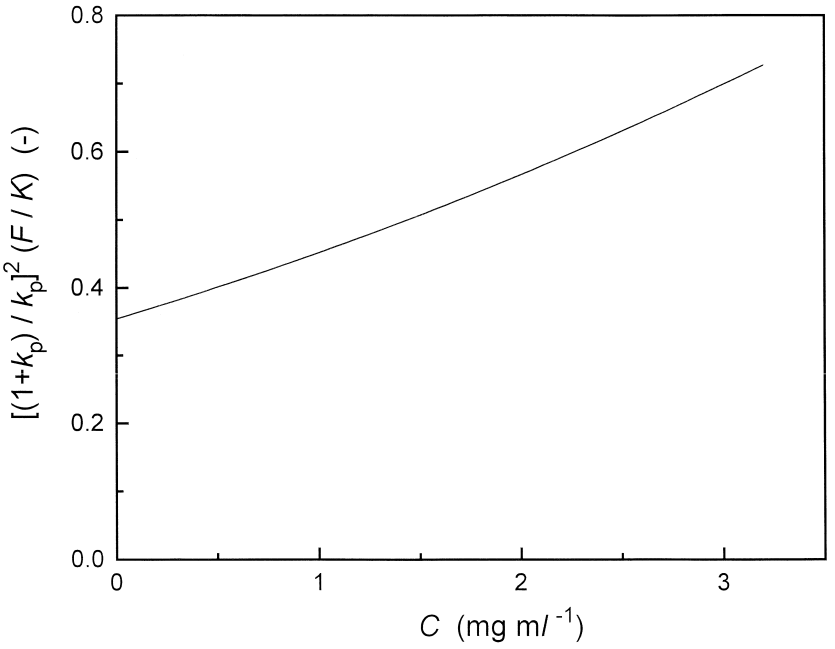

Fig. 10. Plot of $[(1+k_p)/k_p]^2(F/K)$ as a function of the *S*-TB concentration.

term in the RHS of Eq. (22), i.e., $([1+k_p]/k_p)^2(F/K)$, is plotted against *C*. The value of $([1+k_p]/k_p)^2(F/K)$ increases with increasing *C*. The profile in Fig. 10 resembles the relationship between k_m (inversely proportional to the equilibrium constant) and *C* that is shown in Fig. 3, suggesting that the positive dependence of k_m on the *S*-TB concentration can be explained by the characteristics of the phase equilibrium. A significant concentration dependence of D_e and D_s was not observed in the system used in this study. This situation is different from those previously studied in RPLC [34] and in anion-exchange chromatography [18,19].

4.7. Analysis of thermodynamic properties of the mass transfer of S-TB in CTA

Jacobson et al. [6] measured the profiles of the elution peaks of the two enantiomers of TB on CTA under linear isotherm conditions while changing the flow-rate of the mobile phase, ethanol, and the temperature. From the temperature dependence of k' and k_m, they calculated the adsorption enthalpy (ΔH_{ads}) and the overall activation energy for the mass transfer of *S*-TB (E_{total}) as -20.1 kJ mol^{-1} and 49.3 kJ mol^{-1}, respectively. Seidel-Morgenstern and Guiochon [5] reported an almost identical value for ΔH_{ads}. These authors [5,6] pointed out that E_{total} was 2.5-times larger than $-\Delta H_{ads}$ and suggested that the kinetics of adsorption–desorption or of the formation of the chiral discrimination complex (whatever the chiral retention mechanism may be) had an important contribution to the band broadening. In this study, an attempt was made to interpret the thermodynamic properties of the mass transfer phenomena of *S*-TB in the CTA column.

As predicted by Eqs. (8) and (9), k_m is correlated with the four kinetic parameters, i.e., k_f, D_p, D_s, and k_{ads}. The temperature dependence of k_m probably results from those of these four parameters. In this study, E_{total} is assumed to consist of the individual contributions of each mass transfer process and that these contributions are additive.

$$E_{total} = E_f + E_d + E_r \quad (23)$$

where E_{total} is the overall activation energy determined from the temperature dependence of k_m, and E_f, E_d, and E_r are the contributions of the fluid-to-particle mass transfer kinetics, the intraparti-

cle diffusion, and the adsorption/desorption to E_{total}, respectively.

First, the contribution of the fluid-to-particle mass transfer (E_f) is probably negligible because of the quite small contribution of this process to the overall mass transfer resistance. By contrast, the data in Fig. 9 predict that E_d and E_r have comparable contributions to E_{total}. Second, E_d might be estimated from the two contributions of the pore diffusion (E_p) and the surface diffusion (E_s). Because D_p is estimated using Eq. (10), E_p would be equal to the activation energy of the molecular diffusion (E_m), which is derived from Eq. (19) to be 17.4 kJ mol^{-1} for the migration of *S*-TB in ethanol. Alternately, it can be derived from the restricted molecular diffusion model proposed in a previous paper [34] as an approximation of the surface diffusion process. Surface diffusion was regarded as molecular diffusion restricted by the additional adsorptive interactions between the solute and the surface of the stationary phase. The restricted molecular diffusion model was formulated on the basis of the absolute rate theory. The value of E_s is divided into two contributions, those of a hole-making step (E_h) and a jumping step (E_b)

$$E_s = E_h + E_b \tag{24}$$

In this model, a hole is first formed by the removal of the proper number of solvent molecules located in the potential field of adsorption. Then, the solute molecule transfers from a neighbor adsorption site into this hole. The value of E_h is probably correlated with the evaporative energy of the solvent. From considerations based on the absolute rate theory, E_h was shown to be almost equal to E_m. The transfer of the solute molecule into the hole is assumed to require the gain of a certain amount of activation energy, which is necessary for breaking the adsorption interactions between the solute molecule and the surface of the stationary phase. The value of E_b should be correlated with the adsorption enthalpy (ΔH_{ads}). On the basis of these considerations, the following equation was derived.

$$E_s = E_m + \beta(-\Delta H_{ads}) \tag{25}$$

The activation energy of surface diffusion (E_s) is the sum of the activation energy of molecular diffusion (E_m) and of the contribution of the adsorption interactions, represented by $\beta(-\Delta H_{ads})$. The value of β was determined to be as about 0.4 for surface diffusion in RPLC [34]. If we take this value (0.4) for β in the phase system of the TB enantiomeric separation, E_s is calculated to be 25.4 ($=17.4+0.4\times20.1$) kJ mol^{-1}. Because the contributions of pore and surface diffusions to intraparticle diffusion are almost the same in the low concentration range, as illustrated in Fig. 7, the contribution due to the intraparticle diffusion (E_d) in Eq. (23) is roughly estimated to be 21.4 kJ mol^{-1}, the average of E_p (17.4 kJ mol^{-1}) and E_s (25.4 kJ mol^{-1}).

Finally, E_r was estimated by analyzing the experimental data reported by Seidel-Morgenstern et al. [8]. These authors studied the band broadening of TB in the CTA (d_p: 15–25 μm)–ethanol phase system by means of staircase frontal analysis and determined the adsorption isotherms and the column efficiency in nonlinear chromatography at three different temperatures (30, 40, and 50°C). The column efficiency increased with increasing concentration of *S*-TB on the whole at each temperature. The positive concentration dependence of the column efficiency was analyzed to estimate k_{ads}, the temperature dependence of which provides E_r. The contribution of the first term in the RHS of Eq. (16) ($A=2D_L/u$) to H was subtracted in order to calculate k_m from H at each *S*-TB concentration by Eqs. (16) and (17). Eq. (2) is rearranged at $K_a=0$ as follows.

$$H = \frac{2D_L}{u} + 2\left(\frac{F\epsilon_p}{1+F\epsilon_p}\right)^2\left[\frac{ud_p}{6Fk_f} + \frac{ud_p^2}{60FD_p}\right] \tag{26}$$

The two parameters, i.e., k_f and D_p, included in Eq. (26) were estimated from Eqs. (10), (18) and (19). For the CTA column, the value of $2D_L/u$ was calculated as $2.3\cdot10^{-2}$ cm from the HETP measured with tri-*tert*.-butylbenzene (unretained) at the flow-rate of 0.5 ml min^{-1}. As in Fig. 4, k_{ads} was estimated from the plot of $F/(Kk_m)$ versus $1/K$. Fig. 11 shows the Arrhenius plot of the values of k_{ads} thus obtained, with

$$\frac{d\ln k_{ads}}{d(1/T)} = \frac{-E_r}{R} \tag{27}$$

where R is the universal gas constant. The value of

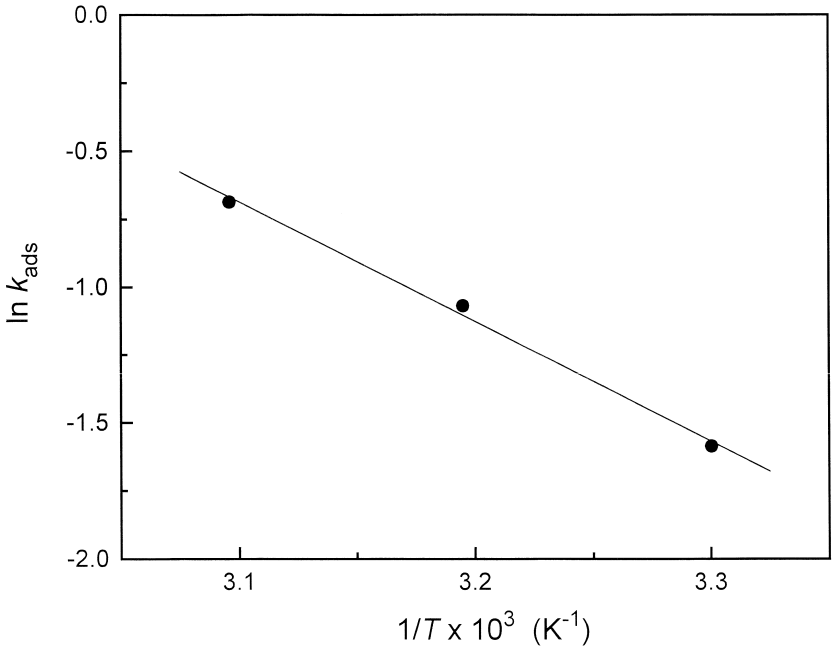

Fig. 11. Arrhenius plot of k_{ads}.

k_{ads} at 40°C is calculated to be 0.34 s^{-1} in Fig. 11, which is very close to the value of k_{ads} estimated in Fig. 4, i.e., 0.42 s^{-1} (through the linear regression) or 0.56 s^{-1} (through the second-order regression). From the slope of the straight line in Fig. 11, E_r is estimated as 36.7 kJ mol^{-1}. From these values of E_d (21.4 kJ mol^{-1}) and E_r (36.7 kJ mol^{-1}), E_{total} is calculated to be 58.1 kJ mol^{-1}. This value is comparable with the one reported by Jacobson et al. [6], i.e., 49.3 kJ mol^{-1}. Although these two values are not identical, the agreement may be considered as quite satisfactory considering the degree of approximation in the estimate of some of the parameters involved. In conclusion, this work shows that a reasonable interpretation of the overall activation energy of the mass transfer of *S*-TB in the CTA column can be obtained from the analysis of the individual contributions of each of the individual kinetic processes.

5. Conclusions

This reevaluation of the experimental results previously published concerning the mass transfer kinetics of *S*-TB in its enantiomeric separation led to some important conclusions. First, the main kinetic parameters, i.e., D_e, D_p, D_s, and k_{ads}, characterizing the main mass transfer processes inside the CTA particles, i.e., intraparticle diffusion and the kinetics of adsorption/desorption, could be calculated by analyzing the concentration dependence of k_m. Second, the contributions of each mass transfer process to the band broadening could be calculated using the kinetic parameters so estimated. Irrespective of the concentration range of *S*-TB, intraparticle diffusion played an important role in the overall mass transfer resistance at high flow-rate range. However, the concentration dependence of D_e and D_s was found to be small. The value of D_s decreased slightly with increasing concentration of *S*-TB. The kinetics of the adsorption/desorption process influences also the characteristics of the concentration dependence of k_m. The slightly positive concentration dependence of k_m seemed to be explained by the same trend of the adsorption/desorption process, which itself was due to the nonlinear behavior of the phase equilibrium. A quantitative interpretation of the activation energy measured for the mass transfer

of *S*-TB in the CTA column showed that the analysis of the kinetics of each transport process involved in the CTA column provides information on the characteristic features of the mass transfer resistance and the thermodynamic properties.

These results explained why excellent agreement was observed between the experimental profiles under strongly nonlinear conditions [4] and those calculated from the equilibrium isotherms with the equilibrium-dispersive model. The column efficiency was poor for the TB enantiomers (ca. 120 theoretical plates) but this was mainly due to slow dispersion, which is properly accounted for in the model, not to a slow mass transfer kinetics, which would not be. Finally, the contrast between the low column efficiency observed for the TB enantiomers and the high efficiency for water (ca. 5000 theoretical plates) justifies neglecting the contributions to the band profile originating from the lack of radial homogeneity of the column packing [41], an effect which would invalidate all similar studies carried out with chromatographic systems giving narrower peaks.

6. List of symbols

- a, Langmuir parameter (–)
- A, Coefficient in Eq. (16) (–)
- b, Langmuir parameter (ml mg^{-1})
- C, Concentration of the solute in the mobile phase (mg ml^{-1})
- C_s, Concentration of the solute adsorbed on the stationary phase (mg ml^{-1})
- C_s', Defined in Eq. (17) (s)
- C_s^*, C_s in equilibrium with C (mg ml^{-1})
- d_p, Particle diameter (cm)
- D_a, Apparent axial dispersion coefficient (cm^2 s^{-1})
- D_e, Intraparticle diffusivity (cm^2 s^{-1})
- D_L, Axial dispersion coefficient (cm^2 s^{-1})
- D_m, Molecular diffusivity (cm^2 s^{-1})
- D_p, Pore diffusivity (cm^2 s^{-1})
- D_s, Surface diffusion coefficient (cm^2 s^{-1})
- E, Activation energy (kJ mol^{-1})
- E_b, Activation energy of the jumping step (kJ mol^{-1})
- E_h, Activation energy of the hole-making step (kJ mol^{-1})
- E_m, Activation energy of the molecular diffusion (kJ mol^{-1})
- E_p, Activation energy of the pore diffusion (kJ mol^{-1})
- E_s, Activation energy of the surface diffusion (kJ mol^{-1})
- F, Phase ratio $[=(1-\epsilon_T)/\epsilon_T]$ (–)
- H, Height equivalent to a theoretical plate (cm)
- ΔH_{ads}, Adsorption enthalpy (kJ mol^{-1})
- H_{Pe}, Defined in Eq. (14) (–)
- H_{St}, Defined in Eq. (15) (–)
- k_{ads}, Adsorption rate constant (s^{-1})
- k_f, External mass transfer coefficient (cm s^{-1})
- k_m, Mass transfer rate coefficient representing the contributions of the fluid-to-particle mass transfer, the intraparticle diffusion, and the adsorption/desorption to the band broadening (s^{-1})
- $k_{m,L}$, Lumped mass transfer rate coefficient representing the contributions of the axial dispersion, the fluid-to-particle mass transfer, the intraparticle diffusion, and the adsorption/desorption to the band broadening (s^{-1})
- k_p, Defined in Eq. (2b) (–)
- k', Retention factor (–)
- k_0', Retention factor at infinite dilution (–)
- k_1, Defined in Eq. (2a) (–)
- K, Partition coefficient in nonlinear chromatography $[=FK_a=F(\Delta q/\Delta C)]$ (–)
- K_a, Adsorption equilibrium constant (–)
- L, Column length (cm)
- M, Molecular weight (–)
- N, Number of the theoretical plates (–)
- Pe, Peclet number (–)
- q, Concentration of the solute in the stationary phase (mg ml^{-1})
- q_s, Saturated amount adsorbed (mg ml^{-1})
- r_A, Stokes radius of *S*-TB (nm)
- r_p, Pore radius of CTA (nm)
- R, Gas constant (J mol^{-1} K^{-1})
- Re, Reynolds number (–)
- S_A, Surface area of CTA (m^2 g^{-1})
- Sc, Schmidt number (–)
- S_F, Swelling factor (–)
- Sh, Sherwood number (–)
- St, Stanton number (–)
- t, time (s)

- T, Absolute temperature (K)
- u, Average interstitial velocity of the mobile phase (cm s^{-1})
- V_b, Molar volume at the normal boiling point (cm^3 mol^{-1})
- V_p, Pore volume of CTA (cm^3 g^{-1})
- V_0, Hold-up volume of the column (ml)
- z, Longitudinal distance along the column (cm)

6.1. Greek symbols

- α_A, Association coefficient in Eq. (19) (–)
- β, Ratio of E_b to $-\Delta H_{ads}$ (–)
- δ, Mass transfer resistance (s)
- ϵ, Void fraction of the column (–)
- ϵ_p, Intraparticle porosity (–)
- ϵ_T, Total porosity of the column (–)
- η, Viscosity (Pa s)
- θ, Surface coverage (–)
- λ, Hindrance parameter (–)
- τ, Tortuosity factor (–)

6.2. Subscripts

- ax, Contribution of the axial dispersion
- d, Contribution of the intraparticle diffusion
- f, Contribution of the fluid-to-particle mass transfer
- r, Contribution of the adsorption/desorption
- s, *S*-TB
- sv, Solvent
- total, Overall

Acknowledgements

This work was supported in part by Grant CHE-97-01680 of the National Science Foundation and by the cooperative agreement between the University of Tennessee and the Oak Ridge National Laboratory.

References

[1] G. Blaschke, J. Liq. Chromatogr. 9 (1986) 341.
[2] T. Shibata, I. Okamoto, K. Ishii, J. Liq. Chromatogr. 9 (1986) 313.
[3] E. Francotte, A. Junker-Bucheit, J. Chromatogr. 576 (1992) 1.
[4] A. Seidel-Morgenstern, G. Guiochon, Chem. Eng. Sci. 48 (1993) 2787.
[5] A. Seidel-Morgenstern, G. Guiochon, J. Chromatogr. 631 (1993) 37.
[6] S.C. Jacobson, A. Seidel-Morgenstern, G. Guiochon, J. Chromatogr. 637 (1993) 13.
[7] P. Rearden, P. Sajonz, G. Guiochon, J. Chromatogr. A 813 (1998) 1.
[8] A. Seidel-Morgenstern, S.C. Jacobson, G. Guiochon, J. Chromatogr. 637 (1993) 19.
[9] H. Guan-Sajonz, P. Sajonz, G. Zhong, G. Guiochon, Biotechnol. Prog. 12 (1996) 380.
[10] P. Sajonz, H. Guan-Sajonz, G. Zhong, G. Guiochon, Biotechnol. Prog. 13 (1997) 170.
[11] P. Sajonz, M. Kele, G. Zhong, B. Sellergren, G. Guiochon, J. Chromatogr. A 810 (1998) 1.
[12] B. Al-Duri, G. McKay, J. Chem. Tech. Biotechnol. 55 (1992) 245.
[13] S.J. Gibbs, A.S. Chu, E.N. Lightfoot, T.W. Root, J. Phys. Chem. 95 (1991) 467.
[14] K. Lederer, I. Amtmann, S. Vijayakumar, J. Billiani, J. Liq. Chromatogr. 13 (1990) 1849.
[15] W.H. Gallagher, C.K. Woodward, Biopolymer 28 (1989) 2001.
[16] R.L. Marlowe, H.E. Jackson, Spectrosc. Lett. 23 (1990) 1203.
[17] G. Guiochon, S. Golshan-Shirazi, A.M. Katti, Fundamentals of Preparative and Nonlinear Chromatography, Academic Press, Boston, MA, 1994.
[18] K. Miyabe, G. Guiochon, Biotechnol. Progr., in press.
[19] K. Miyabe, G. Guiochon, in preparation.
[20] A.M. Katti, G. Guiochon, Adv. Chromatogr. 31 (1991) 1.
[21] L. Lapidus, N.R. Amundson, J. Phys. Chem. 56 (1952) 984.
[22] J.J. van Deemter, F.J. Zuiderweg, A. Klinkenberg, Chem. Eng. Sci. 5 (1956) 271.
[23] D.M. Ruthven, Principles of Adsorption and Adsorption Processes, Wiley, New York, 1984.
[24] M. Suzuki, Adsorption Engineering, Kodansha/Elsevier, Tokyo, 1990.
[25] H. Koller, K.H. Rimböck, A. Mannschreck, J. Chromatogr. 282 (1983) 89.
[26] R. Isaksson, P. Erlandsson, L. Hansson, A. Holmberg, S. Berner, J. Chromatogr. 498 (1990) 257.
[27] A.M. Rizzi, J. Chromatogr. 478 (1989) 71.
[28] E.J. Wilson, C.J. Geankopolis, Ind. Eng. Chem. Fundam. 5 (1966) 9.
[29] R.C. Reid, J.M. Prausnitz, T.K. Sherwood, The Properties of Gases and Liquids, McGraw-Hill, New York, 1977.
[30] R.E. Treybal, Mass Transfer Operations, McGraw-Hill, New York, 1980.
[31] A.M. Rizzi, J. Chromatogr. 478 (1989) 87.
[32] D.D. Frey, E. Schweinheim, C. Horváth, Biotechnol. Prog. 9 (1993) 273.
[33] I.H. Park, C.S. Johnson Jr., D.A. Gabriel, Macromolecules 23 (1990) 1548.
[34] K. Miyabe, G. Guiochon, Adv. Chromatogr. 40 (1999), in press.

[35] R.G. Bogar, J.C. Thomas, J.B. Callis, Anal. Chem. 56 (1984) 1080.
[36] A.L. Wong, J.M. Harris, J. Phys. Chem. 95 (1991) 5895.
[37] S.L. Zulli, J.M. Kovaleski, X.R. Zhu, J.M. Harris, M.J. Wirth, Anal. Chem. 66 (1994) 1708.
[38] R.L. Hansen, J.M. Harris, Anal. Chem. 67 (1995) 492.
[39] R.D. Tilton, C.R. Robertson, A.P. Gast, J. Colloid Interface Sci. 137 (1990) 192.
[40] H. Yoshida, M. Yoshikawa, T. Kataoka, AIChE J. 40 (1994) 2034.
[41] T. Farkas, M. Sepaniak, G. Guiochon, AIChE J. 43 (1997) 1964.